

# Material characterization of the encapsulation of an ultrasound contrast microbubble and its subharmonic response: Strain-softening interfacial elasticity model

Shirshendu Paul, Amit Katiyar, and Kausik Sarkar

*Department of Mechanical Engineering, University of Delaware, Newark, Delaware 19716*

Dhiman Chatterjee

*Department of Mechanical Engineering, IIT Madras, Chennai, 600036 India*

William T. Shi<sup>a)</sup> and Flemming Forsberg

*Department of Radiology, Thomas Jefferson University, Philadelphia, Pennsylvania 19107*

(Received 25 November 2009; revised 5 April 2010; accepted 5 April 2010)

Two nonlinear interfacial elasticity models—interfacial elasticity decreasing linearly and exponentially with area fraction—are developed for the encapsulation of contrast microbubbles. The strain softening (decreasing elasticity) results from the decreasing association between the constitutive molecules of the encapsulation. The models are used to find the characteristic properties (surface tension, interfacial elasticity, interfacial viscosity and nonlinear elasticity parameters) for a commercial contrast agent. Properties are found using the ultrasound attenuation measured through a suspension of contrast agent. Dynamics of the resulting models are simulated, compared with other existing models and discussed. Imposing non-negativity on the effective surface tension (the encapsulation experiences no net compressive stress) shows “compression-only” behavior. The exponential and the quadratic (linearly varying elasticity) models result in similar behaviors. The validity of the models is investigated by comparing their predictions of the scattered nonlinear response for the contrast agent at higher excitations against experimental measurement. All models predict well the scattered fundamental response. The nonlinear strain softening included in the proposed elastic models of the encapsulation improves their ability to predict subharmonic response. They predict the threshold excitation for the initiation of subharmonic response and its subsequent saturation. © 2010 Acoustical Society of America. [DOI: 10.1121/1.3418685]

PACS number(s): 43.80.Qf, 43.25.Yw, 43.40.Ga, 43.35.Mr [CCC]

Pages: 3846–3857

## I. INTRODUCTION

Intravenously injected gas-filled microbubbles (typical diameter  $<10 \mu\text{m}$ ) have been approved as ultrasound contrast agents for cardiovascular imaging in the United States, Europe and elsewhere. They are also actively being investigated for imaging of other organs such as liver, kidney and brain and have been approved for such applications in Europe and elsewhere.<sup>1</sup> A free bubble with a radius of  $1 \mu\text{m}$  lasts in water for 30 ms.<sup>2</sup> Contrast microbubbles derive their stability against dissolution from the protective encapsulation made of proteins (human serum albumin for Optison, GE Healthcare, Princeton, NJ), lipids (SonoVue, Bracco, Geneva, Switzerland; Definity, Lantheus Medical Imaging, N. Billerica, MA; Sonazoid, GE Healthcare, Oslo, Norway) and surfactants (Imavist, Alliance Pharmaceuticals, San Diego, CA). However, the encapsulation also affects the scattering response of the bubbles. A proper characterization of the encapsulation and its relationship with the scattering function therefore are critical for design of new and improved contrast agents. Following up on our recent investigations of encapsulation,<sup>3,4</sup> this paper proposes two new non-

linear viscoelastic models for the bubble encapsulation, apply them to find the properties of the encapsulation of a commercial contrast agent (Sonazoid), and investigate its subharmonic response.

Although several models have been developed to describe the effects of encapsulation on bubble dynamics, the physics remains incompletely understood.<sup>3–18</sup> The earliest models by de Jong and co-workers used parameters—shell friction and shell elasticity—to characterize the encapsulation. Church<sup>12</sup> developed the first detailed theoretical model of the encapsulation as a layer of incompressible rubbery material with linear bulk constitutive viscosity and elasticity. He performed a theoretical analysis using a perturbation method without relating the model to any specific contrast microbubble. Nonetheless, Hoff *et al.*<sup>19</sup> and many subsequent studies<sup>4,20</sup> used this model to investigate and analyze *in vitro* experiments of contrast microbubbles. A major concern about the model lies in its assumption of incompressibility and material homogeneity of the encapsulating layer. Biochemical analysis<sup>21–23</sup> reveals the encapsulation often to be a monolayer, or at most a few-molecules-thick, which is therefore neither homogeneous nor isotropic. The model due to Church or its modification due to Hoff *et al.*<sup>19</sup> also requires a value for the thickness of the layer. Furthermore, the constitutive equation for the encapsulation in this model is

<sup>a)</sup>Present address: Phillips Research North America, Briarcliff Manor, New York.

based on the assumption of small deformation which might not be appropriate for the large radius change experienced at stronger excitations e.g., those giving rise to a subharmonic response.

In 2003, we proposed a zero-thickness interface model with intrinsic interfacial rheology (stress-strain relation) for the encapsulation.<sup>3</sup> For a bubble size ( $\sim\mu\text{m}$ ) far larger than the thickness ( $\sim\text{nm}$ ) of the encapsulation, such a zero-thickness interface model is appropriate, and it avoids prescription of the encapsulation thickness and any specific assumption about the bulk material of the encapsulation. In that paper, a two-pronged approach for rigorous material characterization was proposed—finding the model parameters through one (attenuation) experiment, and an independent validation against a second (nonlinear scattering) experiment. The simplest rheology—Newtonian interface with a dilatational interfacial viscosity ( $\kappa^s$ ) and a surface tension ( $\gamma_0$ )—was adopted. The attenuation of ultrasound measured through a solution of the contrast agent was used to find the encapsulation properties. The parametrized model was then validated against a second measurement, scattered harmonic and non-harmonic responses. Applying the Newtonian model (NM) to a number of different commercial contrast agents predicted unusually high values of surface tension ( $\gamma_0 \sim 0.7\text{--}40\text{ N/m}$ ) compared to the uncontaminated air-water interface value ( $0.07\text{ N/m}$ ). Yet the model predicted the experimentally observed subharmonic response very well for the contrast agent Optison. The unphysical value of surface tension insinuated a non-Newtonian rheology for the interface with an explicit interfacial elasticity  $E^s$ . The constituent surface active molecules in the encapsulation are in close association with each other giving rise to a solid like interface rather than a Newtonian fluid like interface. Indeed introduction of elasticity in a viscoelastic model [referred to as the constant elasticity model (CEM)] led to a reasonable value of surface tension ( $\gamma_0 \sim 0.02\text{ N/m}$ ) for Sonazoid bubbles.<sup>4</sup> Also both the NM and the CEM predict the same value for the dilatational viscosity ( $\sim 10^{-8}\text{ N s/m}$ ), as expected, because introducing elasticity should not change the viscous component. Despite such welcome features, the CEM failed when judged for its ability to predict subharmonic response. In fact, the Newtonian model with its large unphysical surface tension value fared far better in predicting the threshold for and the level of the subharmonic response than the CEM and a modified version of Church's model due to Hoff *et al.*<sup>19</sup> The failure was attributed to the linear model of interfacial elasticity which presumably does not correctly describe the large oscillation that generates the subharmonic response. Consequently, here we pursue a nonlinear extension of our viscoelastic model.

Constitutive modeling of material behavior is a difficult task especially for a nanometer thick encapsulation. Here the simplest extensions of the linear Hooke's law—a quadratic elasticity model (QEM) (interfacial elasticity varying linearly with area fraction) and an exponential elasticity model (EEM) (elasticity varying exponentially)—are adopted. A linear viscoelastic model due to Marmottant *et al.*<sup>13</sup> is also considered. These authors give an elegant description of the elasticity arising from the change in surface tension with the

bubble area. The model results in an expression of the elasticity, which is the same as our constant elasticity model in the linear regime. However, their model is linear only within a range with lower and upper limits—a buckling radius below which the encapsulation buckles with the surface tension becoming zero, and a rupture radius above which the encapsulation breaks and the surface tension assumes the value of an uncontaminated air-water interface. Determination of these radii is not easy, but reasonable values of parameters were shown to predict well the temporal dynamics of a microbubble radius, including a “compression only behavior” where a contrast microbubble compresses more than it expands. Such behavior was experimentally observed for SonoVue bubbles.<sup>13,24</sup> Following our investigation of a constant elasticity model of Sonazoid,<sup>4</sup> constitutive models appropriate for membranes such as Mooney-Rivlin (strain-softening) and Skalak (strain-hardening) models were applied to the encapsulation of contrast microbubbles, where the authors performed a parametric investigation of the effects of the various constitutive parameters on the response of a bubble surrounded by such membranes.<sup>25</sup> These models have been widely used for membranes of capsules and biological cells,<sup>26,27</sup> that contain incompressible liquid in contrast to the compressible gas in a microbubble, and therefore do not undergo volume change. Membrane models (e.g., Mooney-Rivlin model for rubbery material) find the membrane stresses using the generalized strain energy, which is a function of the invariants of the finite deformation membrane strains. Different functional forms of the strain energy give rise to different nonlinear constitutive laws for the membrane including strain softening and hardening.<sup>27</sup> Skalak *et al.*<sup>28</sup> proposed a specific form of nonlinear strain energy function for the membrane of the red blood cells, which has an almost incompressible area; the form is chosen to incorporate the experimental result that “a change of shape at constant area requires relatively small stresses as compared with the stresses required to increase the area of the membrane.” Therefore, it is unclear if such specialized membrane constitutive laws are appropriate for the microbubble encapsulation. Moreover, for the radial oscillation of microbubbles (in contrast to shape deformation of capsules), where area fraction is the only relevant parameter, such general models are not necessary, and using them lead to difficulty in explaining the underlying physics. A Maxwell model appropriate for a “fluid like” membrane (in contrast to a “solid like” membrane where Kelvin's model is more appropriate) with extensions to nonlinear viscosity have also been applied to the modeling of the bubble encapsulation.<sup>14,15</sup>

In this paper, the ultrasound attenuation through a microbubble solution and a linearized Rayleigh-Plesset type model are used to determine the characteristic properties of the encapsulation of Sonazoid bubbles. Our previous measurement with these bubbles is used. The behaviors of different models for this contrast agent are investigated in detail by varying frequency and excitation levels. Then the full nonlinear bubble dynamics model is applied to predict the fundamental and subharmonic responses for various frequencies and compared to measurement.

## II. MATHEMATICAL FORMULATION

### A. Interfacial rheological models for encapsulations

Viscoelasticity is introduced in the constant elasticity model (CEM) using a surface dilatational elasticity term  $E^s$  in the following way:<sup>4</sup>

$$E^s = \left( \frac{\partial \gamma}{\partial \beta} \right)_{\beta=0}, \quad \gamma = \gamma_0 + E^s \beta, \quad (1)$$

where  $\beta = dA/A = [(R/R_E)^2 - 1]$  is the fractional change in area from unstrained position (radius  $R_E$ ), and  $\gamma_0$  is the reference surface tension at that unstrained position. Note that this formulation is identical to the one in the model due to Marmottant *et al.*<sup>13</sup> in the linear regime. However, one could introduce surface elasticity as an independent property without relating it to the surface tension (see the discussion in Ref. 29). If it is related to the surface tension, one might impose a condition of non-negativity on the surface tension<sup>29</sup>

$$\gamma(R) = \begin{cases} \gamma_0 + E^s \left[ \left( \frac{R}{R_E} \right)^2 - 1 \right] & \text{for } \gamma_0 + E^s \left[ \left( \frac{R}{R_E} \right)^2 - 1 \right] > 0 \\ 0 & \text{for } \gamma_0 + E^s \left[ \left( \frac{R}{R_E} \right)^2 - 1 \right] \leq 0. \end{cases} \quad (2)$$

However, if dilatational elasticity is introduced as an independent property, the first line in Eq. (2) suffices, as is used in Ref. 4. The interfacial stress gives rise to a jump in the normal stress at the interface (see Ref. 27 for a detailed derivation). In the present spherically symmetric problem, it appears as a pressure jump: The dynamic boundary condition at the gas-liquid interface becomes

$$p_{r=R} = P_G - 4\mu \frac{\dot{R}}{R} - \frac{4\kappa^s \dot{R}}{R^2} - \frac{2\gamma_0}{R} - \frac{2E^s}{R} \left[ \left( \frac{R}{R_E} \right)^2 - 1 \right], \quad (3)$$

where  $p_{r=R}$  is the pressure in the surrounding liquid just outside the bubble,  $P_G$  is the gas pressure inside the bubble; because motion inside the bubble is neglected, inside stress is the isotropic hydrostatic pressure. Moreover,  $\mu$  is the viscosity of the surrounding liquid, and  $\kappa^s$  denotes the surface dilatational viscosity. The second term in the right-hand-side is due to the viscous normal stress in the liquid. The last three terms are the interfacial stresses due to dilatational viscosity, surface tension and surface dilatational elasticity, respectively. In the case of a Newtonian interface,  $E^s = 0$ . Note that if the non-negativity is not imposed, and dilatational elasticity is independently introduced, Eq. (3) might lead to a net compressive stress on the interface. Such a state will induce Euler type buckling in the encapsulation,<sup>26,27</sup> as seen for encapsulated bubbles.<sup>30</sup> Wrinkled bubbles were shown to bind better to their target site.<sup>31</sup> However, to accurately describe the buckling behavior, encapsulation rheology needs a bending resistance term. For the present purpose, where only spherical dynamics is considered, it suffices to assume that there is a finite bending resistance that determines the right wrinkling behavior, which, however, does not play any role in the spherical dynamics.<sup>26</sup> In this paper, models with and without the constraint of non-negativity imposed on the sur-

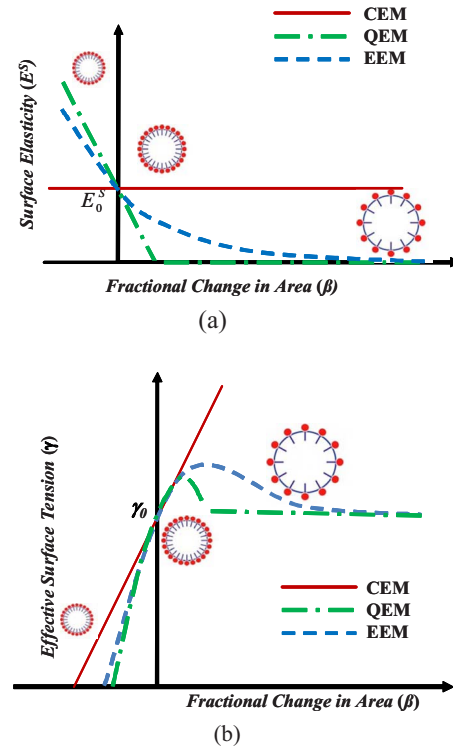


FIG. 1. (Color online) A representative figure depicting the change of interfacial elasticity with fractional change of area for constant (CEM), quadratic (QEM), and exponential (EEM) elasticity models.

face tension will be considered. The model with a non-negative effective surface tension is denoted with (NN).<sup>32</sup>

In the rest state ( $\dot{R}(t=0)=0$ ), nominally the inside pressure  $P_G$  is higher than the outside pressure by the Laplace term  $2\gamma_0/R$ . However, for an elastic encapsulation, there exists a possibility of an equilibrium rest state  $P_{G0}=P_0$ , where a compressive elastic stress in a compressed interface exactly balances the surface tension. Such a state is critical for long time stability of a contrast microbubble.<sup>2,29</sup> Another possibility is that the surface tension is zero at the initial area ( $\gamma(R_0)=0$ ), which is the case for the Marmottant model if  $R_0=R_{\text{buckle}}$  because the model assumes  $\gamma(R \leq R_{\text{buckle}})=0$ .<sup>13</sup> The elastic stabilization in our model results in

$$R_E = R_0 \left( 1 - \frac{\gamma_0}{E^s} \right)^{-1/2}. \quad (4)$$

Below, two models for variation in the surface dilatational elasticity  $E^s$  are introduced: the quadratic elasticity model and the exponential elasticity model.

#### 1. QEM

As the area fraction increases, the constituent molecules in the encapsulation are distended from their close packed conformation. As a result the encapsulation elasticity reduces. The consequent strain-softening can be modeled by a linearly varying elasticity (Fig. 1)

$$E^s = \begin{cases} E_0^s - E_1^s \beta & \text{for } E_0^s - E_1^s \beta > 0 \\ 0 & \text{for } E_0^s - E_1^s \beta < 0, \end{cases} \quad (5)$$

where  $E_0^S$  and  $E_1^S$  are characterization parameters to be determined. The second condition ensures that the elasticity remains positive (unlike the effective surface tension, negative

elasticity would result in an unphysical behavior). The dynamic boundary condition at bubble interface (3) then is replaced by

$$p_{r=R} = \begin{cases} P_G - 4\mu \frac{\dot{R}}{R} - \frac{4\kappa^S \dot{R}}{R^2} - \frac{2\gamma_0}{R} - \frac{2\beta}{R}(E_0^S - \beta E_1^S) & \text{for } E_0^S - E_1^S \beta > 0 \\ P_G - 4\mu \frac{\dot{R}}{R} - \frac{4\kappa^S \dot{R}}{R^2} - \frac{2\gamma_0}{R} & \text{for } E_0^S - E_1^S \beta < 0 \end{cases} \quad (6)$$

Imposing the condition of pressure equilibrium ( $P_{G0} = P_0$ ) at the initial zero motion state obtains a quadratic equation for  $\beta_0$  (initial area fraction). Solving it, one obtains

$$R_E = R_0 \left( 1 + \frac{E_0^S - \sqrt{(E_0^S)^2 + 4\gamma_0 E_1^S}}{2E_1^S} \right)^{-1/2}, \quad (7)$$

where the initial equilibrium radius is chosen to be smaller than the unstrained radius (the correct root of the quadratic equation) so that the resulting compressive strain balances the surface tension leading to a pressure equilibrium.

## 2. EEM

Quadratic model (5) introduces an abrupt change in elasticity to ensure positive dilatational elasticity. With the increasing area fraction, the progressive loss of elasticity could be better modeled by an exponential decay (Fig. 1)

$$E^s = E_0^s \exp(-\alpha^s \beta), \quad (8)$$

with  $\alpha^s$  and  $E_0^s$  to be determined. As before, using dynamic boundary condition at the rest state and imposing  $P_{G0} = P_0$ , one obtains

$$\frac{2\gamma_0}{R_0} + \frac{2E_0^s}{R_0} \beta_0 \exp(-\alpha^s \beta_0) = 0. \quad (9)$$

Linearizing it for a small value of  $\beta_0$  obtains a quadratic equation similar to the quadratic model above.  $R_E$  is given by Eq. (7) for QEM, when  $E_1^s$  is replaced with  $\alpha^s E_0^s$  as follows:

$$R_E = R_0 \left[ 1 + \left( \frac{1 - \sqrt{1 + 4\gamma_0 \alpha^s / E_0^s}}{2\alpha^s} \right) \right]^{-1/2}. \quad (10)$$

## B. Encapsulated bubble dynamics

Motion of the liquid surrounding the bubble is governed by the following equation:

$$\rho \left( R\ddot{R} + \frac{3}{2}\dot{R}^2 \right) = p_{r=R} - P_0 + p_A(t) - \frac{R}{c} \frac{dP_G}{dt}, \quad (11)$$

where  $P_0$  is the hydrostatic pressure,  $c$  is the sound speed and  $p_A(t)$  is the excitation pressure. Dynamic boundary condition (3) at the bubble interface provides  $p(r=R)$ . Note that in contrast to the incompressible form of the equation used in

Ref. 4 here the first-order compressibility effect is incorporated following Ref. 33. Introduction of compressibility changes the characteristic parameter values for the encapsulation by less than 1%. However, compressibility may affect the nonlinear dynamics. The gas pressure inside the bubble is assumed to follow a polytropic gas law  $P_G R^{3k} = P_{G0} R_0^{3k}$  with the polytropic constant  $k=1$ , which strictly corresponds to isothermal behavior; for typical contrast agent content  $k$  is close to unity even for adiabatic processes ( $k=1.066$  for  $C_4F_{10}$ ,  $k=1.033$  for  $SF_6$ ).

Using Eq. (11) along with the appropriate dynamic boundary condition, one obtains the following Rayleigh-Plesset type equation:

$$\rho \left( R\ddot{R} + \frac{3}{2}\dot{R}^2 \right) = P_{G0} \left( \frac{R_0}{R} \right)^{3k} \left( 1 - 3k \frac{\dot{R}}{c} \right) - 4\mu \frac{\dot{R}}{R} - \frac{4\kappa^S \dot{R}}{R^2} - \frac{2\gamma_0}{R} - \frac{2E^s}{R} \left[ \left( \frac{R}{R_E} \right)^2 - 1 \right] - P_0 + p_A(t), \quad (12)$$

with initial conditions  $R(t=0) = R_0$ , and  $\dot{R}(t=0) = 0$ .  $E^s$  is either a constant (CEM) or given for different (QEM or EEM) models by Eq. (5) or Eq. (8). Note that the nature of excitation [shape of  $p_A(t)$ ] has been found to critically affect the scattered response. Simulations in Ref. 4 were performed with a sinusoidal pulse having a Gaussian envelope modulating the amplitudes of 64 cycles. Here a sinusoidal pulse consisting of 64 cycles of constant amplitude, which is closer to what was used in the experiment, is used. A specific encapsulation is characterized by values of the parameters for each model ( $\gamma_0, \kappa^s, E^s$ ) for viscoelastic rheology with constant elasticity,  $\gamma_0, \kappa^s, E_0^s, E_1^s$  for the quadratic model and  $\gamma_0, \kappa^s, E_0^s, \alpha^s$  for the exponential model. To obtain scattering cross-section, the system is solved using a stiff solver (ODE15s) in MATLAB<sup>®</sup> (Mathworks Inc., Natick, MA). The total scattering cross-section

$$S_s(\omega) = \int_{R_{\min}}^{R_{\max}} \sigma_s(R; \omega) n(R) dR \quad (13)$$

is obtained from the simulated scattered pressure  $P_s(t)$  as follows:<sup>4</sup>

$$\sigma_s(r, t) = \frac{4\pi \langle r^2 P_s(r, t)^2 \rangle}{P_A^2}, \quad P_s(r, t) = \rho \frac{R}{r} (2\dot{R}^2 + R\ddot{R}). \quad (14)$$

$n(R)dR$  is the number of bubbles per unit volume with radius in the range  $(R, R+dR)$ , and the range of bubble radii is given by  $(R_{\min}, R_{\max})$ . The angular brackets indicate average over a time period. Frequency content is determined using Fourier transform.

### C. Determination of characterization parameters using attenuation

The attenuation of ultrasound measured through a diluted Sonazoid solution reported in Ref. 4 is used to deter-

mine the characteristic parameters pertaining to each model. The experiment was performed at low excitation level (as the classical linear theory of attenuation being invalid at higher excitations<sup>34</sup>). Therefore, one can linearize the nonlinear bubble dynamics, Eq. (12), to obtain a harmonic oscillator equation for periodic excitation  $p_A(t) = P_A \sin \omega t$ . The procedure is similar to what was reported in Ref. 4. From the oscillator equation, one can readily obtain the resonance frequency  $\omega_0$  and damping  $\delta$  for each model. They are

$$\begin{aligned} \omega_0^2 &= \frac{1}{\rho R_0^2} \left[ 3kP_0 - \frac{4\gamma_0}{R_0} + \frac{4E^s}{R_0} \right], \\ &= \frac{1}{\rho R_0^2} (3kP_0 + \xi), \quad \xi = 4 \left( 1 + \frac{E_0^s - \sqrt{(E_0^s)^2 + 4\gamma_0 E_1^s}}{2E_1^s} \right) \left( \frac{\sqrt{(E_0^s)^2 + 4\gamma_0 E_1^s}}{R_0} \right), \\ &= \frac{1}{\rho R_0^2} \left[ 3kP_0 + \frac{2E_0^s}{R_0} \left( \frac{\eta}{\alpha^s} \right) (1 + 2\alpha^s - \eta) \right], \quad \eta = \sqrt{1 + \frac{4\gamma_0 \alpha^s}{E_0^s}}, \end{aligned} \quad (15)$$

respectively for the CEM, QEM and EEM. The damping term  $\delta$  is the same for all three models

$$\delta = \frac{1}{\rho \omega_0 R_0^2} \left( 4\mu + 4 \frac{\kappa^s}{R_0} + \frac{3kP_{G0}R_0}{c} \right). \quad (16)$$

One can see that the first term in Eq. (16) is the damping due to the surrounding liquid, the second due to the interface, and the last due to radiation.<sup>3,4</sup> Note that in contrast to Refs. 3 and 4, where the incompressible Rayleigh-Plesset equation was used, here the introduction of compressibility automatically obtains the radiation damping term which is slightly different from the classical expression  $\delta_{\text{radiation}} = \omega^2 R_0 / \omega_0 c$ . The extinction cross-section  $\sigma_e$  for the linearized dynamics is given by<sup>4,35</sup>

$$\sigma_e = 4\pi R_0^2 \frac{c\delta}{\omega_0 R_0} \frac{\Omega^2}{[(1 - \Omega^2)^2 + \Omega^2 \delta^2]}, \quad \Omega = \frac{\omega_0}{\omega}, \quad (17)$$

giving rise to attenuation  $\theta(\omega)$  in dB/distance

$$\theta(\omega) = 10 \log_{10} e \int_{R_{\min}}^{R_{\max}} \sigma_e(R; \omega) n(R) dR, \quad (18)$$

where  $e$  is the base of natural logarithm,  $n(R)dR$  is the number of bubbles per unit volume with radius in the range  $(R, R+dR)$ , and the range of bubble radii is given by  $(R_{\min}, R_{\max})$ . Knowing the bubble properties and the discretized size distribution, this integral can be evaluated. Sonazoid has a relatively narrow size distribution with an average mean diameter of  $3.2 \pm 0.2 \mu\text{m}$  with a number concentration of  $0.78 \pm 0.38$  billions/ml.<sup>36</sup> We have used both the radius distribution<sup>37</sup> as well as the average radius value obtaining essentially the same characteristic values for

the encapsulation. To find the characteristic parameters pertaining to a model, an error function between the measured attenuation and the model attenuation is used as follows:

$$Er(\gamma_0, \kappa^s, E_0^s, \dots) = \sum_i [\theta(\omega_i) - \theta^{\text{meas}}(\omega_i)]^2. \quad (19)$$

The error function is minimized to obtain the parameters using MATLAB<sup>®</sup>.

## III. RESULTS AND DISCUSSION

### A. Acoustic characterization

The experimental attenuation data previously reported in Ref. 4 are used here for determining the characteristic properties of the bubble encapsulation. It was shown there that the attenuation varies linearly with increasing bubble concentration indicating negligible interactions. Using error minimization (19) we find the properties for different models and report them in Table I. For comparison, we use the same attenuation data to find properties for the model due to Marmottant *et al.*<sup>13</sup> The Marmottant model requires values of the buckling radius  $R_{\text{buckling}}$  and break-up radius  $R_{\text{break-up}}$ . These are hard to determine. Following the original reference (Ref. 13), we take  $R_{\text{buckling}} = R_0$ , and  $R_{\text{break-up}} = 1.5R_{\text{buckling}}$ . Parameter estimation using an actual size distribution or using the average radius value lead to the same parameter values (i.e., within the range of experimental scatter) for Sonazoid. However, using an average radius value, one can achieve attenuation values from model fairly close to the measured data [Fig. 2(a)], while using the actual radius distribution results in a simulated attenuation qualitatively similar to the measured data, but the details remain different [Fig. 2(b)]. One

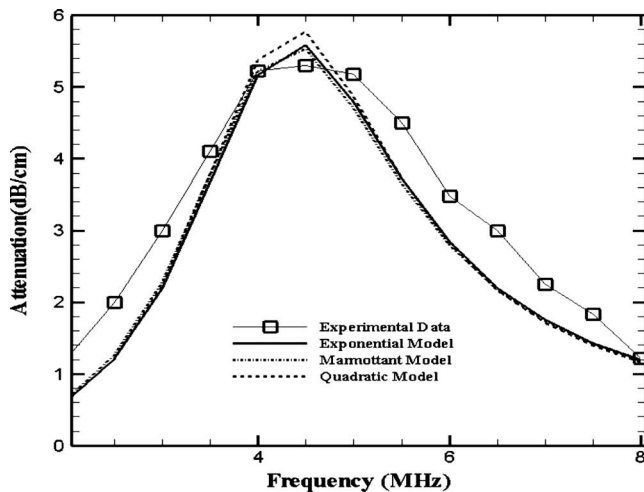
TABLE I. Property values for Sonazoid encapsulation according to various models.

	Quadratic model				Exponential model				Marmottant model			
	$\kappa^s$ ( $\times 10^{-8}$ kg/s)	$\gamma_0$ (N/m)	$E_0^s$ (N/m)	$E_1^s$ (N/m)	$\kappa^s$ ( $\times 10^{-8}$ kg/s)	$\gamma_0$ (N/m)	$E_0^s$ (N/m)	$\alpha$	$\kappa^s$ ( $\times 10^{-8}$ kg/s)	$\chi$ (N/m)	$R_{break-up}$ ...	$R_{buckling}$ ...
Mean	1.2	0.019	0.53	0.75	1.2	0.019	0.55	1.5	1.2	0.53	$1.5R_{buckling}$	Same as initial radius
Range (about mean)	$\pm 0.4$	...	$\pm 0.1$	$\pm 0.015$	$\pm 0.4$	...	$\pm 0.1$	$\pm 0.05$	$\pm 0.4$	$\pm 0.1$	...	...

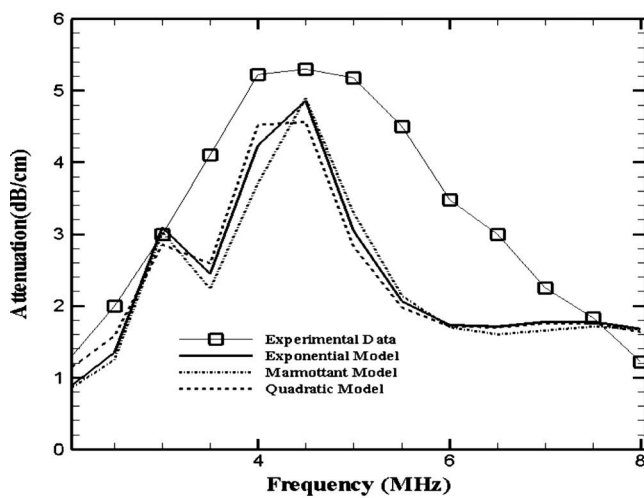
can understand it by assessing the strict constraints of modeling with a complete distribution—bubbles of different radii lead to different dynamics. This also indicates the sensitivity of the radius distribution in finding the property values. Indeed, if one uses a radius distribution that is 10 times less or more than the measured one, the estimation procedure fails—the model cannot give rise to a low error, i.e., close to

measured attenuation for any set of property values. This exercise gives stronger credence to the property determination procedure adopted here.

Table I shows that the value of shell compressibility  $\chi = 0.53$  N/m obtained for the Marmottant model is the same as the surface dilatational elasticity values ( $E^s = 0.53$  N/m for QEM and  $E^s = 0.55$  N/m for EEM) for the elastic models as expected from the fact that the constant elasticity model and the Marmottant model are the same in the linear elastic regime ( $R_{buckling}, R_{break-up}$ ). For QEM (5) and EEM (8), one can also note the consistency condition  $E_1^s(\text{QEM}) \approx \alpha^s E_0^s(\text{EEM})$  being satisfied by the values listed in Table I. Also the value of the surface dilatational viscosity  $\kappa^s$  for the Marmottant model is of the same order as that of the other models. Note that the parameters obtained for the Marmottant model by de Jong and co-workers are of the similar order—van der Meer *et al.*<sup>17</sup> found  $\chi = 0.54 \pm 0.1$  N/m, and  $\kappa^s = 2.3 \times 10^{-8}$  kg/s, Marmottant *et al.*<sup>13</sup> found  $\chi = 1.0$  N/m, and  $\kappa^s = 1.5 \times 10^{-8}$  kg/s, and Gorce *et al.*<sup>16</sup> found  $\chi = 0.55$  N/m, and  $\kappa^s = 0.78 \times 10^{-8}$  kg/s all for SonoVue contrast microbubbles. Below, the fundamental and subharmonic scatterings predicted by different models are investigated comparing them with experimental measurement.



(a)

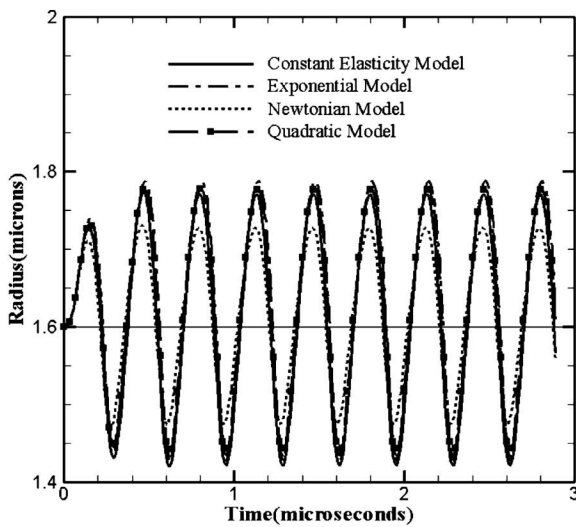


(b)

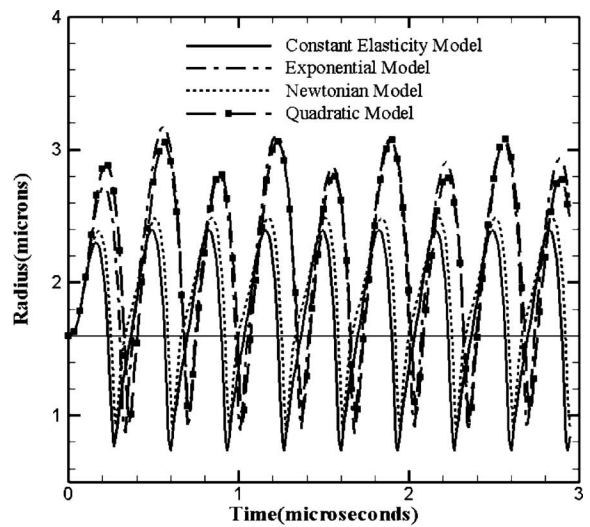
FIG. 2. Measured and fitted attenuation to determine the interface parameters for Sonazoid bubbles according to different models. (a) Parameters estimated with average mean radius and number concentration. (b) Parameters estimated using size distribution. Concentration is 0.103 ml/l of Sonazoid in Isoton II.

## B. Radial dynamics

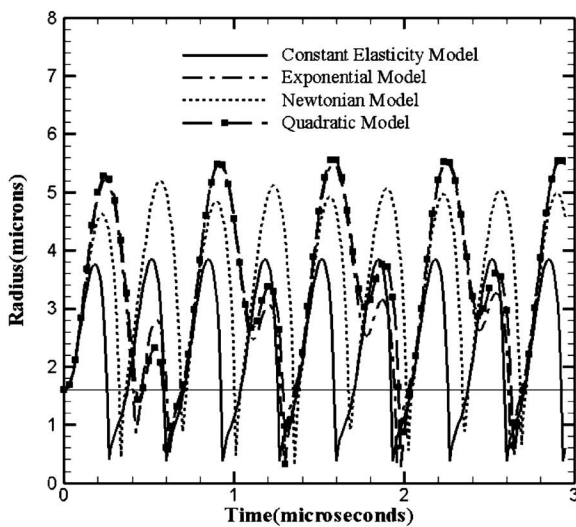
The bubble dynamics, Eq. (12), is solved for an initial radius using the material parameters of the encapsulation (from Table I) to obtain the bubble radius as a function of time. Figure 3 shows them for the constant elasticity (CEM), quadratic (QEM) and the exponential (EEM) elasticity models for varied acoustic excitations (0.1, 0.5, 1.5, and 2.0 MPa) all at 3 MHz. Note that for the lowest level of excitation (0.1 MPa), all curves coincide—for weaker oscillations, the nonlinearity remains inactive. However at higher excitations, the curves for nonlinear viscoelastic models deviate from the constant elasticity one due to the strain softening included in the former models. QEM and EEM show similar behavior for all frequencies and excitation levels. The strain-softening included in the nonlinear models results in larger radial excursions—as the bubble expands, the surface resists expansion with an effectively smaller elasticity modulus. Previously in Ref. 4 we found that unlike the constant elasticity model, a Newtonian model (NM) for the encapsulation fares better in comparing with the measured subharmonic response. To investigate this issue further, the radius vs time curve according to the NM model is also included in Fig. 3. It shows slight deviation relative to the elastic models at 0.1 MPa because of the fundamental difference between the



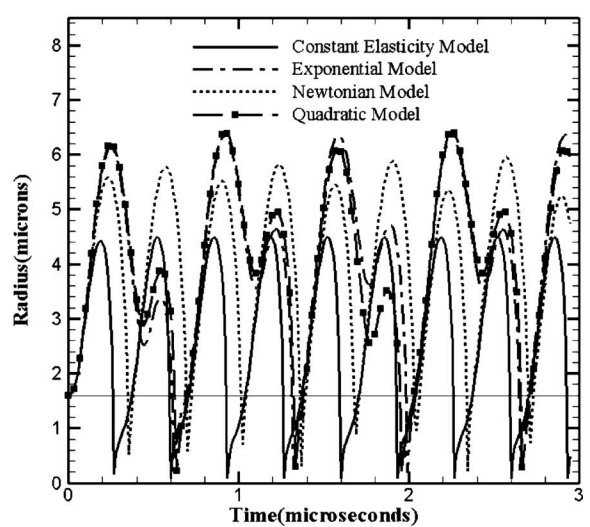
(a)



(b)



(c)



(d)

FIG. 3. Radius-time curves for a  $1.6 \mu\text{m}$  Sonazoid bubble according to different encapsulation  $\mu\text{m}$  models at insonication frequency of 3 MHz and various acoustic pressures (a) 0.1 MPa, (b) 0.5 MPa, (c) 1.5 MPa, (d) 2.0 MPa.

Newtonian and the elastic models. At 0.5 MPa, the radial excursion is smaller than the nonlinear viscoelastic models, but at higher pressures (1.5 and 2.0 MPa), the Newtonian model matches better with the nonlinear models in their amplitude of oscillations. Similar results were found at other ( $\neq 3$  MHz) frequencies (not shown here for brevity). The higher radial excursion for the NM model can explain its better performance in predicting the subharmonic response of a contrast microbubble compared to CEM.

Recently, de Jong and co-workers found that contrast microbubbles experience a “compression only” behavior for the phospholipid coated agents Sonovue and BR14 (Bracco, Geneva, Switzerland), in that the radial excursion away from the equilibrium radius is not symmetric, but the bubble compresses more than it expands.<sup>13,24</sup> The compression only behavior is attributed to the buckled state of the encapsulation below  $R_{\text{buckle}}$ —where the authors assume the surface tension to be zero. As mentioned before, Marmottant *et al.*<sup>13</sup> assumed the same in their model. The rising surface tension

hinders large distension when the bubble expands, but as the bubble compresses into a buckled state, the zero surface tension leads to an asymmetry in dynamics between the expansion and the compression phases. As noted before, in the viscoelastic models proposed here, one can choose to impose the nonnegativity on the surface tension [see Eq. (2)]. On the other hand, surface elasticity could be treated as an independent property, and in that case, the effective surface tension could become negative leading to a net compressive stress. In fact, unlike the case of a zero surface tension in the buckled state, such a net compressive stress can be thought of as a direct cause for buckling of the encapsulation. In Fig. 4, the simulated radial dynamics using the exponential and Marmottant models (the quadratic model’s behavior is similar to the exponential model) are compared. We also include an exponential model, where nonnegativity (NN) has been imposed. Marmottant and the nonnegative exponential models predict very similar results unlike the other exponential model for all cases; they also favor compression only behav-

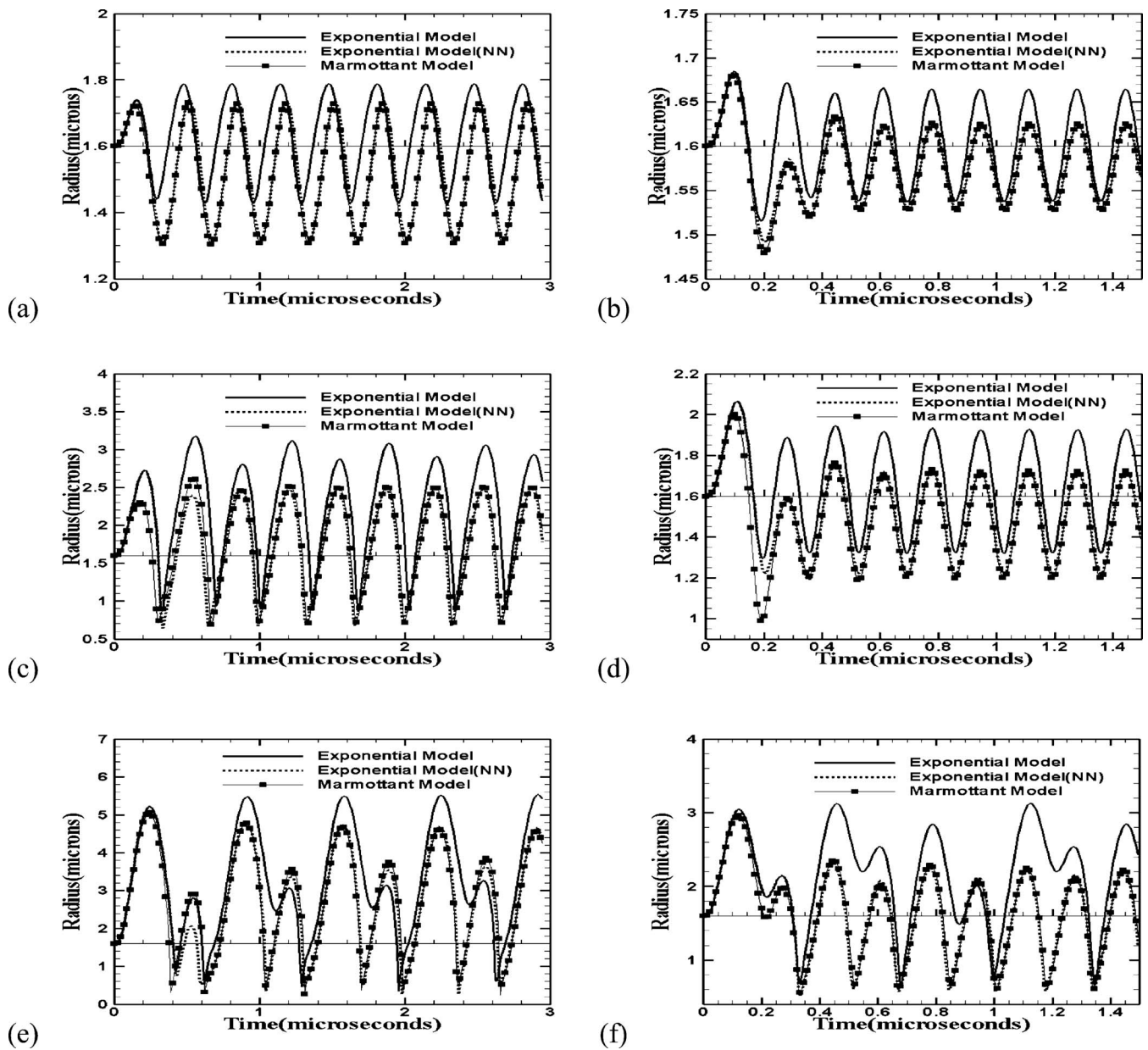


FIG. 4. Radius-time curves for a 1.6  $\mu\text{m}$  Sonazoid bubble according to various models of the encapsulation at different insonication frequencies and acoustic pressures (a) 3 MHz, 0.1 MPa, (b) 6 MHz, 0.1 MPa, (c) 3 MHz, 0.5 MPa, (d) 6 MHz, 0.5 MPa, (e) 3 MHz, 1.5 MPa, (f) 6 MHz, 1.5 MPa.

ior more than the other one. Both at 3 and 6 MHz, one sees a compression only behavior for the Marmottant and the non-negative exponential models but not for the regular exponential model at the acoustic pressure of 0.1 MPa. At 0.5 MPa, compression only behavior is again shown by these two models for 6 MHz but not for 3 MHz. The radial excursion at 3 MHz even for these two models is almost symmetric. At 1.5 MPa excitation, for 3 MHz all curves show larger expansion than compression, and for 6 MHz, the Marmottant and exponential (NN) models predict that bubbles compress marginally more than they expand. According to Ref. 24 compression only behavior is defined as when the maximum expansion to maximum compression is less than 50%. Figure 4 shows that the Marmottant model predicts 85% for this ratio at 6 MHz and 1.5 MPa. Note that the experiments by de

Jong and co-workers showing compression only behaviors for Sonovue and BR14 were performed at lower acoustic pressures  $< 0.25$  MPa.

### C. Scattered fundamental and subharmonic response

The fundamental and subharmonic scattered responses from Sonazoid bubbles were measured and reported for four different frequencies—2, 3, 4.4 and 6 MHz.<sup>4</sup> The scattered fundamental response showed increase with increasing pressure; all models showed similar trends. The subharmonic signal component on the other hand was negligible until a threshold excitation, and then a rapid growth occurred followed by saturation. Plotting the subharmonic data against mechanical index  $MI = P_A / f^{1/2}$  [where  $P_A$  is the acoustic

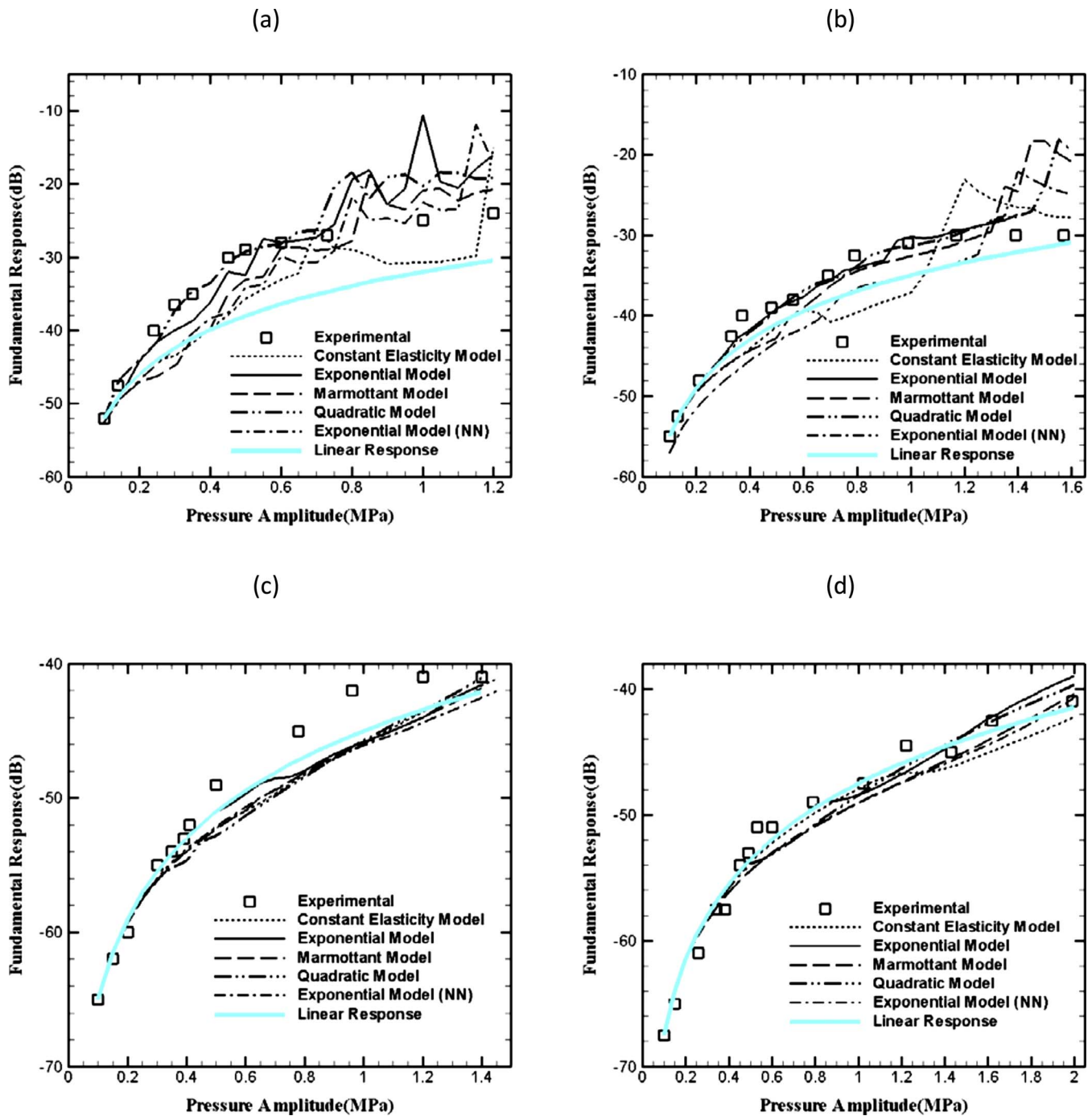


FIG. 5. (Color online) Measured and predicted fundamental response of Sonazoid bubbles at various excitation frequencies: (a) 2 MHz, (b) 3 MHz, (c) 4.4 MHz, (d) 6 MHz.

pressure amplitude measured in MPa and  $f$  is the frequency (MHz)] showed an approximate collapse of the data for different frequencies in that paper.<sup>4</sup>

The scattered response from the radial dynamics is computed using Eq. (14) for scattered pressure. The fundamental and the subharmonic responses are computed using an FFT of the scattered pressure. The model predictions are compared against the same experimental measurements reported in Ref. 4. The experimental data are matched at the lowest excitation level as was also done in Ref. 4 to account for the scattering volume. Figure 5 shows that the fundamental response is modeled very well by all models as was also the

case previously.<sup>4</sup> We have also plotted the response from the linearized system for the EEM model, which matches very well the full nonlinear dynamics except at 2 MHz.

In Fig. 6, the subharmonic response from Sonazoid and the predictions from different models are plotted. As noted before, subharmonic response unlike the fundamental remains negligible until a threshold pressure is exceeded. Each of the models similarly generates no subharmonic response until a threshold excitation. At 2 MHz, all models except the constant elasticity perform well. As was shown before<sup>4</sup> the constant elasticity model (CEM) does not predict the subharmonic response well for any frequency. It fails to predict a

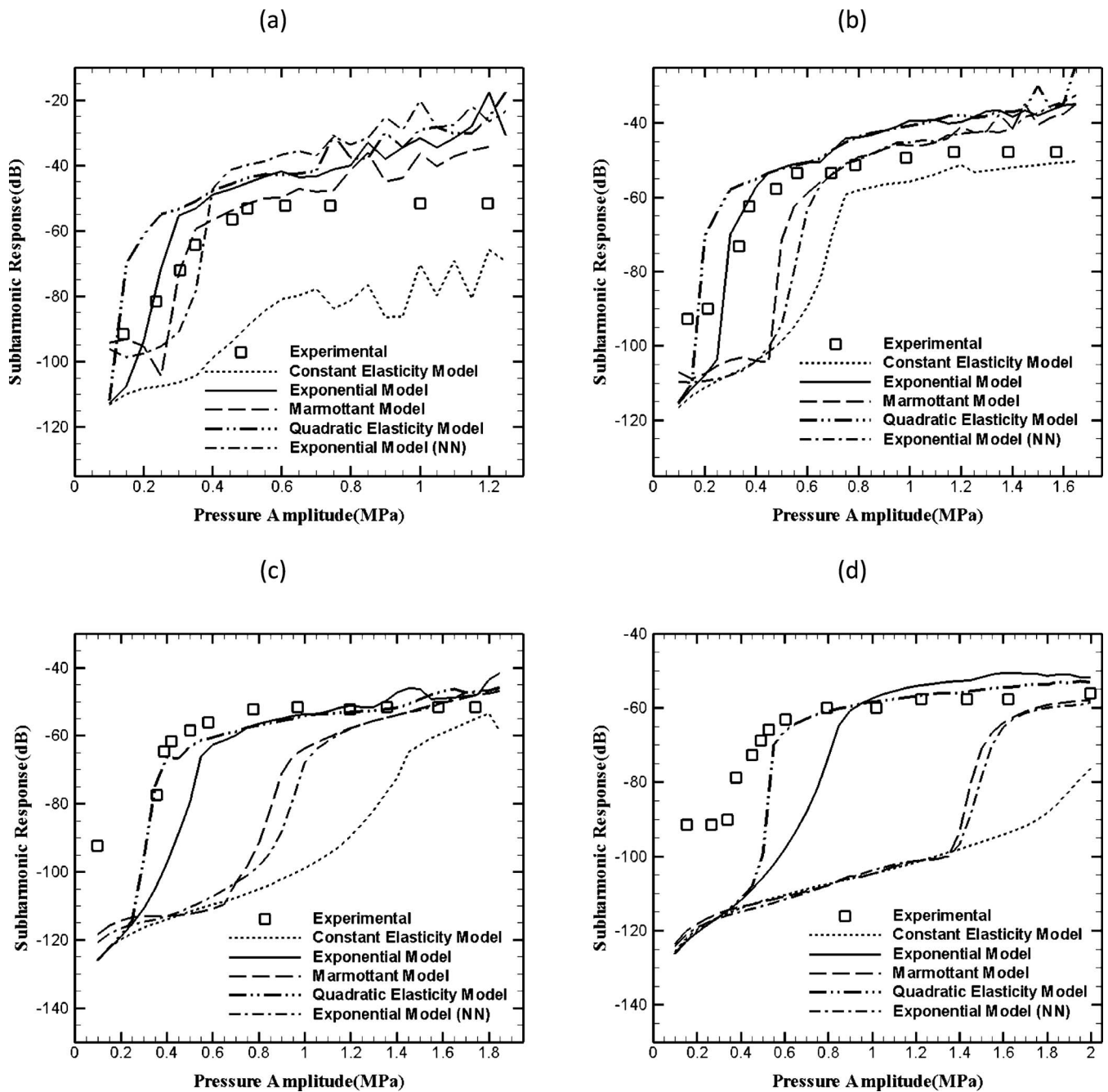


FIG. 6. Measured and predicted subharmonic response of Sonazoid bubbles at various insonication frequencies: (a) 2 MHz, (b) 3 MHz, (c) 4.4 MHz, (d) 6 MHz.

sharp threshold except at 3 MHz, where it predicts a value twice that found in the experiment. The failure of CEM was thought to result from the model's inability to correctly describe the constitutive behavior of the encapsulation for stronger oscillation. As is evident from the plots, other models show a threshold value for subharmonic excitation and predict the saturation level of subharmonic response very well at each of the frequencies. Although the Marmottant model is similar to CEM, it effectively incorporates nonlinearity by prescribing a different behavior above the rupture radius. The threshold values predicted by the different models are listed in Table II. Figure 6 shows that the non-negative exponential model results in a response very similar to the Marmottant model. This can be explained by noting

TABLE II. Threshold pressure (in MPa) for subharmonic scattering obtained experimentally and from different models.

	Frequency (MHz)			
	2	3	4.4	6
Experiments	0.24	0.33	0.36	0.4
CEM	...	0.65	...	...
QEM	0.15	0.20	0.35	0.50
EEM	0.25	0.35	0.45	0.65
EEM (NN)	0.35	0.55	0.90	1.45
Marmottant	0.30	0.50	0.85	1.45

that as the bubble shrinks, both prescribe the surface tension to be zero below a certain value of the bubble radius. The QEM and the EEM perform the best in predicting the experimentally measured threshold values. The Marmottant and the EEM (NN) models predict threshold values higher than the measured ones, especially at the higher frequencies of 4.4 and 6 MHz. Although each of the models predicts greater threshold value at the higher frequencies, the EEM and QEM provide better match with experiment. QEM and EEM are similar in response (see Fig. 3), but QEM model performs better in matching the experimental results at 4.4 and 6 MHz.

#### IV. SUMMARY

Nonlinear models for the encapsulation of a contrast microbubble have been developed and investigated. The encapsulation was treated as a complex interface characterized by constitutive parameters such as surface tension  $\gamma_0$ , dilatational viscosity  $\kappa^s$ , dilatational elasticity  $E_0^s$  and new nonlinearity parameters— $E_1^s$  for the QEM model, where the elasticity decreased linearly with area fraction, and  $\alpha^s$  for the EEM model, where the elasticity varied exponentially. Both nonlinear models represent strain softening resulting from the decreased association between constituent molecules in the encapsulation as its area increases. They resulted in very similar overall response.

The constitutive parameters are key to the mechanical characterization of a specific contrast microbubble agent. In this paper, the parameters associated with a commercial contrast agent Sonazoid were determined (Table I) using measurement of attenuation as a function of frequency. The parameter values pertaining to a recent model due to Marmottant *et al.* were also found for comparison. Different models are consistent in that the values of constitutive parameters arising in them for the same contrast agent can be related to each other. Effects of imposing a constraint of nonnegative effective surface tension (comprising of the reference surface tension and the interfacial elasticity effects) were investigated. The constraint resulted in a behavior very similar to the Marmottant model, because both models prescribe zero surface tension below certain bubble radii. Both (nonnegative exponential and Marmottant) models show compression only behavior at lower acoustic pressures as is observed for certain contrast microbubbles. We have recently shown that effectively non-negative surface tension leads to only neutral stability for an encapsulated contrast bubble against dissolution—as a bubble reaches the compressed state where the surface tension is zero, the bubble does not have any stabilizing force against further shrinking.<sup>32</sup> It therefore can dissolve away by fluctuation.

The models were investigated for their ability to predict the measured nonlinear scattering. Each of the models predicted the fundamental response well. The CEM was shown to perform poorly in predicting the subharmonic response of Sonazoid<sup>4</sup>—it does not predict a threshold value of the acoustic excitation for the subharmonic response seen in experiments. In contrast, introduction of strain softening in QEM and EEM led to the prediction of the threshold value and subsequent saturation. The model due to Marmottant *et*

*al.* also showed a threshold value and saturation, because of its similarity with the nonlinear models presented in this paper. However, the constraint of nonnegativity imposed on it as well as a modified EEM model leads to threshold values significantly higher than the experiment at higher frequencies.

#### ACKNOWLEDGMENTS

K.S. acknowledges support from NSF Grant No. CBET-0651912 and NIH Grant No. P20RR016472. This work is also partially supported by U.S. Army Medical Research Material Command under Grant No. W81XWH-08-1-0503, AHA Grant No. 06554414, and NIH Grant No. HL081892.

- <sup>1</sup>K. Ferrara, R. Pollard, and M. Borden, "Ultrasound microbubble contrast agents: Fundamentals and application to gene and drug delivery," *Annu. Rev. Biomed. Eng.* **9**, 415–447 (2007).
- <sup>2</sup>K. Sarkar, A. Katiyar, and P. Jain, "Growth and dissolution of an encapsulated contrast microbubble," *Ultrasound Med. Biol.* **35**, 1385–1396 (2009).
- <sup>3</sup>D. Chatterjee and K. Sarkar, "A Newtonian rheological model for the interface of microbubble contrast agents," *Ultrasound Med. Biol.* **29**, 1749–1757 (2003).
- <sup>4</sup>K. Sarkar, W. T. Shi, D. Chatterjee, and F. Forsberg, "Characterization of ultrasound contrast microbubbles using in vitro experiments and viscous and viscoelastic interface models for encapsulation," *J. Acoust. Soc. Am.* **118**, 539–550 (2005).
- <sup>5</sup>N. de Jong, F. J. Ten Cate, C. T. Lancée, J. R. T. C. Roelandt, and N. Bom, "Principles and recent developments in ultrasound contrast agents," *Ultrasonics* **29**, 324–330 (1991).
- <sup>6</sup>N. de Jong, L. Hoff, T. Skotland, and N. Bom, "Absorption and scatter of encapsulated gas filled microspheres—Theoretical considerations and some measurements," *Ultrasonics* **30**, 95–103 (1992).
- <sup>7</sup>N. de Jong, R. Cornet, and C. T. Lancée, "Higher harmonics of vibrating gas-filled microspheres. Part one: Simulations," *Ultrasonics* **32**, 447–453 (1994).
- <sup>8</sup>N. de Jong and L. Hoff, "Ultrasound scattering properties of Alunex microspheres," *Ultrasonics* **31**, 175–181 (1993).
- <sup>9</sup>J. S. Allen, D. J. May, and K. W. Ferrara, "Dynamics of therapeutic ultrasound contrast agents," *Ultrasound Med. Biol.* **28**, 805–816 (2002).
- <sup>10</sup>K. E. Morgan, J. S. Allen, P. A. Dayton, J. E. Chomas, A. L. Klibanov, and K. W. Ferrara, "Experimental and theoretical evaluation of microbubble behavior: Effect of transmitted phase and bubble size," *IEEE Trans. Ultrason. Ferroelectr. Freq. Control* **47**, 1494–1509 (2000).
- <sup>11</sup>D. B. Khismatullin and A. Nadim, "Radial oscillations of encapsulated microbubbles in viscoelastic liquids," *Phys. Fluids* **14**, 3534–3557 (2002).
- <sup>12</sup>C. C. Church, "The effects of an elastic solid-surface layer on the radial pulsations of gas-bubbles," *J. Acoust. Soc. Am.* **97**, 1510–1521 (1995).
- <sup>13</sup>P. Marmottant, S. van der Meer, M. Emmer, M. Versluis, N. de Jong, S. Hilgenfeldt, and D. Lohse, "A model for large amplitude oscillations of coated bubbles accounting for buckling and rupture," *J. Acoust. Soc. Am.* **118**, 3499–3505 (2005).
- <sup>14</sup>A. A. Doinikov and P. A. Dayton, "Maxwell rheological model for lipid-shelled ultrasound microbubble contrast agents," *J. Acoust. Soc. Am.* **121**, 3331–3340 (2007).
- <sup>15</sup>A. A. Doinikov, J. F. Haac, and P. A. Dayton, "Modeling of nonlinear viscous stress in encapsulating shells of lipid-coated contrast agent microbubbles," *Ultrasonics* **49**, 269–275 (2009).
- <sup>16</sup>J. M. Gorce, M. Arditi, and M. Schneider, "Influence of bubble size distribution on the echogenicity of ultrasound contrast agents—A study of SonoVue (TM)," *Invest. Radiol.* **35**, 661–671 (2000).
- <sup>17</sup>S. M. van der Meer, B. Dollet, M. M. Voormolen, C. T. Chin, A. Bouakaz, N. de Jong, M. Versluis, and D. Lohse, "Microbubble spectroscopy of ultrasound contrast agents," *J. Acoust. Soc. Am.* **121**, 648–656 (2007).
- <sup>18</sup>D. Chatterjee, P. Jain, and K. Sarkar, "Ultrasound-mediated destruction of contrast microbubbles used for medical imaging and drug delivery," *Phys. Fluids* **17**, 100603 (2005).
- <sup>19</sup>L. Hoff, P. C. Sontum, and J. M. Hovem, "Oscillations of polymeric microbubbles: Effect of the encapsulating shell," *J. Acoust. Soc. Am.* **107**, 2272–2280 (2000).

- <sup>20</sup>M. Emmer, A. Van Wamel, D. E. Goertz, and N. De Jong, "The onset of microbubble vibration," *Ultrasound Med. Biol.* **33**, 941–949 (2007).
- <sup>21</sup>C. Christiansen, H. Kryvi, P. C. Sontum, and T. Skotland, "Physical and biochemical-characterization of Alunex(TM), a new ultrasound contrast agent consisting of air-filled albumin microspheres suspended in a solution of human albumin," *Biotechnol. Appl. Biochem.* **19**, 307–320 (1994).
- <sup>22</sup>A. H. Myrset, H. Nicolaysen, K. Toft, C. Christiansen, and T. Skotland, "Structure and organization of albumin molecules forming the shell of air-filled microspheres: Evidence for a monolayer of albumin molecules of multiple orientations stabilizing the enclosed air," *Biotechnol. Appl. Biochem.* **24**, 145–153 (1996).
- <sup>23</sup>D. M. El-Sherif and M. A. Wheatley, "Development of a novel method for synthesis of a polymeric ultrasound contrast agent," *J. Biomed. Mater. Res. Part A* **66A**, 347–355 (2003).
- <sup>24</sup>B. Dollet, S. M. van der Meer, V. Garbin, N. de Jong, D. Lohse, and M. Versluis, "Nonspherical oscillations of ultrasound contrast agent-microbubbles," *Ultrasound Med. Biol.* **34**, 1465–1473 (2008).
- <sup>25</sup>K. Tsigliffis and N. A. Pelekasis, "Nonlinear radial oscillations of encapsulated microbubbles subject to ultrasound: The effect of membrane constitutive law," *J. Acoust. Soc. Am.* **123**, 4059–4070 (2008).
- <sup>26</sup>E. Lac, D. Barthes-Biesel, N. A. Pelekasis, and J. Tsamopoulos, "Spherical capsules in three-dimensional unbounded Stokes flows: Effect of the membrane constitutive law and onset of buckling," *J. Fluid Mech.* **516**, 303–334 (2004).
- <sup>27</sup>X. Y. Li and K. Sarkar, "Front tracking simulation of deformation and buckling instability of a liquid capsule enclosed by an elastic membrane," *J. Comput. Phys.* **227**, 4998–5018 (2008).
- <sup>28</sup>R. Skalak, A. Tozeren, R. P. Zarda, and S. Chien, "Strain energy function of red blood-cell membranes," *Biophys. J.* **13**, 245–264 (1973).
- <sup>29</sup>A. Katiyar, K. Sarkar, and P. Jain, "Effects of encapsulation elasticity on the stability of an encapsulated microbubble," *J. Colloid Interface Sci.* **336**, 519–525 (2009).
- <sup>30</sup>M. A. Borden and M. L. Longo, "Dissolution behavior of lipid monolayer-coated, air-filled microbubbles: Effect of lipid hydrophobic chain length," *Langmuir* **18**, 9225–9233 (2002).
- <sup>31</sup>J. J. Rychak, J. R. Lindner, K. Ley, and A. L. Klibanov, "Deformable gas-filled microbubbles targeted to P-selectin," *J. Controlled Release* **114**, 288–299 (2006).
- <sup>32</sup>A. Katiyar and K. Sarkar, "Stability analysis of an encapsulated microbubble against gas diffusion," *J. Colloid Interface Sci.* **343**, 42–47 (2010).
- <sup>33</sup>S. Hilgenfeldt, D. Lohse, and M. Zomack, "Response of bubbles to diagnostic ultrasound: A unifying theoretical approach," *Eur. Phys. J. B* **4**, 247–255 (1998).
- <sup>34</sup>D. Chatterjee, K. Sarkar, P. Jain, and N. E. Schreppler, "On the suitability of broadband attenuation measurement for characterizing contrast microbubbles," *Ultrasound Med. Biol.* **31**, 781–786 (2005).
- <sup>35</sup>K. Sarkar and A. Prosperetti, "Coherent and incoherent-scattering by oceanic bubbles," *J. Acoust. Soc. Am.* **96**, 332–341 (1994).
- <sup>36</sup>P. C. Sontum, J. Ostensen, K. Dyrstad, and L. Hoff, "Acoustic properties of NC100100 and their relation with the microbubble size distribution," *Invest. Radiol.* **34**, 268–275 (1999).
- <sup>37</sup>L. Hoff, *Acoustic Characterization of Contrast Agents for Medical Ultrasound Imaging* (Kluwer Academic, Norwell, MA, 2001).